

Dileptons and Photons from Coarse-Grained Microscopic Dynamics and Hydrodynamics Compared to Experimental Data

P. Huovinen¹, M. Belkacem², P. J. Ellis¹ and J. I. Kapusta¹

¹*School of Physics and Astronomy, University of Minnesota
Minneapolis, MN 55455, USA*

²*Laboratoire de Physique Quantique, Université Paul Sabatier
31062 Toulouse Cedex, France*

(October 27, 2018)

Abstract

Radiation of dileptons and photons from high energy nuclear collisions provides information on the space-time evolution of the hot dense matter produced therein. We compute this radiation using relativistic hydrodynamics and a coarse-grained version of the microscopic event generator UrQMD, both of which provide a good description of the hadron spectra. The currently most accurate dilepton and photon emission rates from perturbative QCD and from experimentally-based hadronic calculations are used. Comparisons are made to data on central Pb-Pb and Pb-Au collisions taken at the CERN SPS at a beam energy of 158 A GeV. Both hydrodynamics and UrQMD provide very good descriptions of the photon transverse momentum spectrum measured between 1 and 4 GeV, but slightly underestimate the low mass spectrum of e^+e^- pairs, even with greatly broadened ρ and ω vector mesons. Predictions are given for the transverse momentum distribution of dileptons.

PACS 25.75.-q, 13.85.Qk

I. INTRODUCTION

The primary rationale for colliding large nuclei at high energy is to produce high-density matter in as large a volume as possible for as long as possible. The energy density of atomic nuclei sets the scale at $0.15 \text{ GeV}/\text{fm}^3$. The energy density in neutron stars may reach two to ten times that number. The energy density for the phase transition or crossover from hadronic to quark and gluon degrees of freedom is about ten times that number. In terms of temperature, the phase transition or crossover should occur between 150 and 200 MeV in net-baryon-free matter. A first principles theoretical description of the space-time evolution of the produced matter is not yet possible. It is very much more complicated than lattice quantum chromodynamics (QCD) calculations of the thermodynamic properties. There are only a few well-developed dynamical models of high energy nuclear collisions which provide a space-time description of matter. Chief among these are UrQMD (Ultra relativistic Quantum Molecular Dynamics) [1,2] and relativistic, non-viscous, perfect fluid dynamics, simply referred to as hydrodynamics [3]. UrQMD is restricted to hadronic degrees of freedom, while hydrodynamics can, as here, employ an equation of state which includes both quark-gluon and hadronic phases. Both of these models require input that is not obtainable from experimental data on hadron-hadron collisions and is not yet computable from QCD. In the case of UrQMD one must estimate unmeasured or unmeasurable cross sections, usually involving hadron resonances like the Δ or the ρ . There are also difficulties in dealing with hadron-hadron collisions at high density, for instance in the treatment of off-mass-shell effects and simultaneous collisions of more than two particles. In the case of hydrodynamics one does not know the initial conditions very well, and there is some difficulty in determining when the transition from local thermal equilibrium to free-streaming particles occurs. Nevertheless, sufficient work has been done on these problems to achieve good, theoretically acceptable descriptions of the abundances of different types of hadrons and their momentum distributions for heavy ion collisions at the CERN SPS using both approaches [1,3,4].

The distribution of observed hadrons does not readily provide information on the state of matter prior to their last scattering. It was suggested long ago that the emission of direct photons (those not arising from the decay products of unstable hadron resonances after freezeout) and dileptons (e^+e^- and/or $\mu^+\mu^-$) would provide information on the temperature and baryon density of the evolving matter. The reason is that these electromagnetic probes generally have mean free paths that are much greater than the spatial dimensions of the system. Calculations of the emission rates have become very sophisticated, and there is now essentially a consensus on their magnitudes. For recent reviews see Peitzmann and Thoma [5] and Rapp and Wambach [6]. However, in order to use these thermal emission rates one must know the local temperature and baryon chemical potential as functions of space and time. This is straightforward to obtain in hydrodynamics. To obtain this information in a microscopic event generator, such as UrQMD, one must accumulate an ensemble of collision events and then determine the local variables via coarse-graining. We have done this and will report the results in this paper. The system we focus on is central Pb-Pb collisions at a laboratory beam energy of 158 A GeV, equivalent to a center-of-mass energy of 17 A GeV. The reason we focus on this system is that there is a relative wealth of data taken at the CERN SPS for hadrons, photons, and dileptons. This is not the case at the RHIC (Relativistic Heavy Ion Collider) at Brookhaven National Laboratory where electromagnetic spectra have not yet been measured and only hadron spectra are available.

In Sec. II we compare the space-time evolution of the nuclear collision obtained from hydrodynamics to that obtained from a coarse-graining of UrQMD. In Sec. III we compare the distributions of negatively charged hadrons and net protons from the coarse-grained UrQMD to experimental data, just to be sure that the coarse-graining has not severely distorted the model predictions. In Secs. IV and V we compare the results of these two dynamical models to experimental data on photons and dileptons, respectively. We summarize our results in Sec. VI.

II. SPACE-TIME EVOLUTION

The initial conditions for the hydrodynamic calculation cannot be framed in terms of two colliding nuclei since the primary particle production is a non-adiabatic process which is not describable by perfect fluid dynamics. Instead the hydrodynamic calculation begins with estimated initial conditions soon after impact which are constrained to reproduce the final observed hadron spectra. The UrQMD does begin with the two nuclei approaching each other; strings are formed and decay, producing particles that subsequently rescatter according to hadron-hadron cross sections determined independently. We do not attempt to coarse-grain the initial stage of the collision when many strings are present. Rather, we begin after most or all of the strings have decayed.

The coarse-graining of 100 UrQMD central Pb-Pb collisions is performed in terms of the following variables: proper time $\tau = \sqrt{t^2 - z^2}$, space-time rapidity $\eta = \frac{1}{2} \ln [(t + z)/(t - z)]$, cylindrical radius r , and azimuthal angle ϕ . The origin of the time axis is chosen to be the time when the colliding nuclei overlap. A grid of small space-time cells is set up. Using an ensemble of 100 events, the average total momentum, energy, and net baryon number in each cell is easily found. This allows us to determine the velocity of the center-of-momentum, the energy density, and the baryon density for each cell. A table with the equation of state of an ideal hadron gas containing the same hadronic degrees of freedom as UrQMD is then used to determine the equivalent temperature and baryon chemical potential for each cell. This equation of state is very similar to that obtained in UrQMD without strings [7]. (Inclusion of strings violates the principle of detailed balance unless the back reactions, involving the collision of many particles to reform a string, are included and this is not technically possible at present.) This procedure is justified in our case since the coarse-graining is done after most or all strings have already disappeared, as already mentioned. As shown in the next section this procedure does not severely distort the final hadron spectra.

Our hydrodynamical model has been described in detail in Refs. [3,8]. To keep our dilepton results comparable with the results shown in [9], we use the same equation of state

with a first order phase transition to a quark-gluon plasma at a temperature of $T_c = 200$ MeV, in net baryon free matter, which is at the high end of the range of expected critical temperatures. The parametrization of the initial state is also the same, namely, IS1 from Ref. [8].

The version of hydrodynamics applied here does not assume boost invariance. Therefore a comparison of the space-time evolution with UrQMD has the ambiguity of fixing the zero of time. In the following figures and discussion we have taken $t = 0$ to be the time at which we initialize hydrodynamics and estimate that this corresponds to 0.5 fm/c after the complete overlap of the two nuclei in UrQMD.

When comparing hydrodynamics to the coarse-grained UrQMD we shall focus for the most part on the central ($z = 0$) transverse plane. In Fig. 1 we plot the temperature as a function of local time in a small volume centered at the origin. The effect of the phase transition on the equation of state used by hydrodynamics can be seen at a time around 2 fm/c. The equation of state from UrQMD uses hadronic degrees of freedom only; thus high temperature here means a superheated resonance gas. The two curves in Fig. 1 are remarkably similar, although the evolution in UrQMD is somewhat slower in the sense that the matter takes a longer time to cool. Cooling in the transverse plane is displayed as a contour plot in Fig. 2. It shows the contours of constant temperature in a slice of the $t - r$ plane centered at $z = 0$. Note that the small wiggles arise from the coarse graining of the UrQMD with a finite number of events. The two models yield curves which are qualitatively similar, but once again it is apparent that the matter described by UrQMD takes longer to cool. The most likely explanation is that the matter evolution described by UrQMD dynamics includes the effects of viscosity and heat conduction which will slow its expansion and cooling.

The baryon chemical potential evolution in a small volume centered at the origin is plotted in Fig. 3. Due to the finite number of events in UrQMD the maximum value of the chemical potential does not occur precisely at the origin. Thus the discrepancy between UrQMD and hydrodynamics in the first few fm/c is more apparent than real. After 5 fm/c

the evolution is evidently quite similar in the two models.

Contours of the radial flow velocity in the central plane are displayed in Fig. 4. Apart from fluctuations in the UrQMD results arising from using a finite number of events in the coarse-graining, the contours are almost identical. A more striking difference is seen in the initial¹ velocity distribution along the beam (or z) axis, displayed in Fig. 5. Whereas in UrQMD this velocity distribution is essentially an outcome of the string dynamics, in hydrodynamics it is an assumed input. The UrQMD velocity profile closely resembles a boost-invariant velocity profile $v = z/\sqrt{\tau^2 + z^2}$ with time $\tau = 0.35$ fm/c except in the region close to the origin, $|z| < 0.4$ fm, where the flow velocity is less than in the boost invariant case. Conversely the hydrodynamic profile is close to the boost invariant one for $\tau = 1.0$ fm/c in the region $|z| < 1.0$ fm, whereas at large z the velocity is smaller than that of a boost-invariant profile. Thus the deviations from boost invariant flow are qualitatively different and the differences in velocity profiles cannot be due to the ambiguity in defining the initial time. It should also be remembered that even if the longitudinal velocity profiles in both models resemble boost invariant flow, the matter distributions do not since they peak at $z = 0$.

We have seen that the two models show a remarkable similarity in the temperature, baryon chemical potential, and transverse flow results near the origin and in the central transverse plane. This is most likely due to the (approximate) boost invariance, an essential feature in high energy collisions. In UrQMD it is a consequence, in some sense, of string dynamics. In hydrodynamics it is a combination of relativity and the assumed initial conditions. The small differences are most likely attributable to the fact that the microscopic

¹The reader is advised to keep in mind the ambiguity in fixing the t -axis as explained before. The UrQMD velocity profile is for $\tau = 0.5$ fm/c, whereas the hydrodynamic profile is for $\sqrt{(t + 0.5)^2 - z^2} = 0.5$ fm/c, where time t is measured from the beginning of the hydrodynamical evolution.

model includes in an essential way the physical effects of shear and bulk viscosity and heat conduction. The similarities are not so striking in the longitudinal direction, which is probably a consequence of the way that finite energy effects are actually implemented in the two dynamical models (exact boost invariance occurs only at infinite beam energy). Nevertheless the similarities are great enough that one may conclude that the UrQMD results in something akin to local thermal equilibrium, at least insofar as we have probed it with the coarse-graining procedure. It would be very interesting and worthwhile to carry out fluid dynamic calculations with the initial conditions obtained from UrQMD, both with and without viscosity and heat conduction included. Such studies are the subject of another paper.

III. HADRON SPECTRA

The initial conditions of hydrodynamics are chosen so that experimental hadronic spectra for Pb-Pb collisions at 158 A GeV are relatively well reproduced [4,8]. The results of UrQMD also reproduce the experimental hadronic spectra quite well, apart from hyperons containing two or three strange quarks which may signal interesting physics not contained in the model [1,10,11].

To investigate whether the coarse-graining distorts the hadronic spectra we have calculated the hadronic spectra from the coarse-grained UrQMD temperature, chemical potential, and flow velocity fields in the same way as in hydrodynamics². When coarse-graining is done on a microscopic model like UrQMD one faces exactly the same issue as in hydrodynamics: when to stop and compute the hadronic spectra. We have generally taken a range of freeze-out temperatures, namely 140, 120, and 100 MeV, and results will be displayed for these cases. For comparison the default temperature at which the hydrodynamic evolution ceases

²The hadronic equation of state used in the hydrodynamic calculations is essentially identical to the equation of state obtained from running UrQMD without strings in a large box.

and free-streaming begins was chosen to be 140 MeV, a value determined in earlier studies [8].

In Fig. 6 we show the rapidity distribution of negatively charged hadrons compared to data taken by the NA49 collaboration [12]. In this and the subsequent figures the top panel shows the UrQMD results which can be compared with the hydrodynamic result in the bottom panel. A freeze-out temperature between 120 and 100 MeV in UrQMD yields the best comparison to the data. The hydrodynamic description fits the data quite nicely since the initial conditions were tuned to this end. The transverse mass distributions at laboratory rapidities of 3.4, 3.9 and 4.4 are shown in Fig. 7. The UrQMD results are acceptable for essentially any freezeout temperature in the range displayed; the hydrodynamic results in the lower panel also agree with the data.

The net proton (proton minus anti-proton) spectra are displayed in Fig. 8. The sensitivity of the UrQMD results to the freeze-out temperature is greater here than it is for the negative hadron spectra. This is understandable since in chemical equilibrium, with a nonzero baryon chemical potential, the ratio of anti-protons to protons is exponentially sensitive to the temperature, behaving approximately as $\exp(-2\mu_B/T)$. This, together with the increased transverse flow velocity as the system evolves to lower temperatures, qualitatively explains the results of Fig. 8. Although a freeze-out temperature of around 140 to 120 MeV might seem to be favored, these results cannot be used to pin down the freeze-out conditions. The reason is that the anti-protons are very sensitive to annihilation processes and to non-equilibrium dynamics in the relatively dilute stage at the end of the collision. Still, considering the extreme assumption of local thermal and chemical equilibrium used to obtain these results, the outcome is reasonable. The hydrodynamic results (lower panel) are quite similar to the UrQMD results when the same freeze-out temperature, 140 MeV, is employed.

Overall we may conclude that the coarse-graining has not severely distorted the original UrQMD results which represent the experimental data well.

IV. PHOTON SPECTRA

The emission of direct photons from nuclear collisions has long been considered a good probe of the temperatures and energy densities achieved. The reason is that the emission rate for photons of energy E is proportional to the Boltzmann factor $\exp(-E/T)$, making photons quite sensitive to the temperature. On the other hand, the absolute number is obtained by integrating over space and time, so large volumes and long lifetimes can compensate for low temperatures. In addition, the rate quoted is in the local rest frame of the hot matter. If this matter is flowing, the photons can be red shifted to lower energy or blue shifted to higher energy. The transverse momentum spectra of photons involves convoluting all of these effects.

To see whether there is a signal of thermal photon emission is very difficult experimentally. Model calculations have shown that thermal emission is expected to be overwhelmed by the decays of hadrons, most notably $\pi^0 \rightarrow \gamma\gamma$. A lengthy and careful analysis of Pb-Pb collisions at 158 A GeV by the WA98 collaboration [13] has produced the photon spectrum shown in Fig. 9. All known hadronic decays into photons have been subtracted. This spectrum is then identified with direct photons only. The curve in the figure is the next-to-leading order pQCD (perturbative QCD) result of photon production from the primary interactions of incoming partons [14] as shown in [15]. In this calculation an intrinsic parton momentum of $\langle k_T^2 \rangle = 0.9 \text{ GeV}^2$ necessary to describe proton-induced reactions at a similar energy is assumed³. Since the photons from primary interactions cannot explain the measured photon yield, the yield must be associated with the secondary interactions of the produced particles. In the following we use the pQCD results shown in Fig. 9. It must be kept in mind that the true pQCD photons could be less than this by a factor of two [15].

³It is shown in [16] that if an additional nuclear broadening $\Delta k_T^2 \simeq 0.5 - 1 \text{ GeV}^2$ is added by hand, the WA98 photon spectrum can be explained above $p_t = 2.5 \text{ GeV}$. However, prompt photons fail to reproduce the data at low $p_t < 2.5 \text{ GeV}$ regardless of the amount of broadening employed.

The comparison between thermal photon emission from hydrodynamic calculations and the WA98 data has been done several times [17,18]; for a review see Ref. [5], for a study of the sensitivity to the initial conditions and the equation of state see Ref. [18]. In our calculations we have applied the rate calculations of Refs. [19–21] in the hadronic phase and the recent complete order- α_s calculation of Ref. [22] in the quark-gluon plasma phase. The results from the hydrodynamic calculation are shown in the lower panel of Fig. 10. Here the pQCD result of Fig. 9 is added to the thermal contribution. The agreement can only be described as excellent. Further, the results show almost no dependence on the freeze-out temperature. As shown in Ref. [18] the reason is that the contribution from the early hot stages of the evolution dominate.

The analogous comparison using the space-time evolution of coarse-grained UrQMD is shown in the upper part of Fig. 10. Again there is hardly any dependence on the freeze-out temperature because the emission from the early hot stage dominates. The photon emission has also been calculated using UrQMD on a microscopic level [23]. A precise comparison with our results cannot be made since the photon production processes are not exactly the same in both cases, nevertheless the yields are quite similar. Even so we caution the reader regarding difficult points in our approach. Firstly, we began the calculation of the thermal photon emission from UrQMD at a proper time of 1 fm/c after complete overlap. There is uncertainty within UrQMD as to how to compute at earlier times when the strings are still fragmenting into hadrons, or viewed differently, how to compute photon emission before the hadrons materialize and are allowed to interact strongly (pre-formation time). This is very subtle, and involves the transition from pQCD reactions to those hadronic interactions included in UrQMD. Secondly, as seen in Fig. 1, the initial temperatures can exceed 200 MeV, but the parametrization of the thermal production rates [20] we employ were fit only in the range $100 < T < 200$. Finally, the pQCD results employed here may overestimate the direct photons. These remarks serve to emphasize the sensitivity of the photon yield to the early high energy density stages of the collision.

V. DILEPTON SPECTRA

The dilepton spectrum measured in Pb-Au collisions is shown in Fig. 11. Instead of the data shown by the CERES collaboration [24] we use the preliminary '95 and '96 data for the most central collisions from the theses of Voigt [25] and Lenkeit [26], respectively. These collisions have the highest energy density which should enhance the interesting physics; this is indeed found to be the case experimentally [26]. It is also necessary to focus on central collisions since our hydrodynamical model assumes cylindrical symmetry and it is tuned to reproduce hadronic data from the most central collisions [12].

This data has generated much excitement since it displays two very interesting features. The first is qualitative: there is no hint of a peak in the ρ - ω mass region. The second is quantitative: there is a large excess of pairs in the mass range $0.25 < M < 0.7$ GeV when compared to expectations based on the decays of hadrons after freezeout, called the “cocktail” or “background” contribution, and represented by the curve in Fig. 11. We use the background estimate from Ref. [26] in all of our calculations here.

The thermal emission rate of dileptons can be computed using many-body theory and the vector meson dominance model for temperatures where the matter can be described in terms of hadronic degrees of freedom. The most complete calculation using medium-unmodified hadrons was done by Gale and Lichard [27,28] and is shown by the solid line in Fig. 12. The two most sophisticated calculations using medium-modified hadrons are shown in the same figure. The calculations performed by Rapp *et al.* [29] are based on solving one loop self-energy diagrams self-consistently for the ρ - π - N complex with interactions determined by low energy physics. The calculations by Eletsky *et al.* [30] are based on scattering amplitudes for the same complex constructed from experimental data, namely, resonances at low energy and Regge amplitudes at high energy. Although the latter two calculations are technically quite different, they aim at the same physics, and the thermal emission rates indicated by the dashed and dotted curves in Fig. 12 are also very similar. This is reassuring; it is very important to understand these rates quantitatively in order to draw conclusions from

experiments performed by the CERES collaboration and other groups. Both of the medium-modified calculations exhibit the behavior indicated by the CERES data: suppression of the ρ - ω peak and enhancement at invariant masses below 650 MeV. The reason is that the ρ and ω mesons become greatly broadened at high energy density, with their strength distributed mostly to lower masses. In the following we use the rates from Eletsky *et al.*, although the rates of Rapp *et al.* would yield essentially the same conclusions.

As with photons, the thermal dilepton radiation from hydrodynamics has been compared to the CERES data several times [6,9,29]. Fig. 13 shows our results, which are computed for Pb-Pb collisions with a freeze-out temperature of 140 MeV. Compared to experiment the medium-unmodified thermal rate (dashed curve) predicts somewhat fewer dileptons in the mass range from 0.3–0.6 GeV, as in Ref. [9]. Some improvement is gained by using the medium-modified rate (solid curve).

Using only the medium-modified rate, and lowering the freeze-out temperature to 120 or 100 MeV helps fill in the intermediate mass region a little, but not quite enough, as shown in the bottom panel of Fig. 14. Going to a lower freeze-out temperature may seem to be undesirable since it tends to enhance the ρ - ω mass region and since it is inconsistent with the value determined from the hadronic spectra. On the other hand, there can still be contributions to dilepton production in the free-streaming hadronic stage. As shown in Ref. [31], if dileptons from those few collisions in the free-streaming stage are added to those coming from the pre-freeze-out stage, the full result is insensitive to the numerical value of the freeze-out temperature. Since we do not attempt to add the free-streaming contribution here, it is perhaps natural to use a somewhat lower freeze-out temperature for the dileptons than for the hadrons.

The upper panel of Fig. 14 shows the results obtained with the coarse-grained UrQMD. They are almost identical to the hydrodynamical results. The slower cooling exhibited by UrQMD might lead one to expect larger dilepton yield, but the difference in cooling rate is too small for any significant difference to build up. However, this effect can be seen when different freeze-out temperatures are compared. UrQMD cools more slowly, especially during

the later stages of evolution, and therefore decreasing the freeze-out temperature increases the lepton yield more in the UrQMD than in the hydrodynamical model. It is also worth noticing that for the momenta discussed here the dilepton yields, unlike the photon yields, are not dominated by the initial hot stage of the evolution. In fact, dilepton emission from the hot $T > 200$ MeV region is a minor correction [9] to the emission from cooler regions.

In order to put these results in perspective we have also binned the calculated dilepton yields in the same way as the experimental data. The results are shown in Fig. 15 and compared to just the '96 data [26]. Both the UrQMD and the hydrodynamic results are within one standard deviation of the data when $T_f = 100$ MeV. The agreement is only slightly worse when $T_f = 140$ MeV. From this viewpoint it would seem premature to decide that there is a discrepancy with theory in the 0.3–0.6 GeV mass range until additional data are available.

There are other calculations of thermal dileptons [9,29,32], but, with the exception of Ref. [9], these calculations were not compared to the most central Au+Pb data. They used data averaged over a larger range of impact parameter, corresponding to $\langle dN/d\eta \rangle = 250$, whereas we compare to data with $\langle dN/d\eta \rangle = 350$. As mentioned before, the many-body effects increase with increasing centrality to a significant degree, particularly in the 0.3–0.6 GeV mass range. Further the results obtained by Rapp *et al.* [29,32] were obtained with a less sophisticated approach than employed here. They used a very simple parametrizations of the space-time evolution of the temperature and flow velocity, essentially spherical fireballs or cylindrical firetubes. They did not compare with the hadronic data, which we view as an important consistency check.

To see if the difference in initial longitudinal velocity profile between UrQMD and hydrodynamics (Fig. 5) leaves any observable signal we calculate the rapidity distributions of dileptons without any acceptance cuts, and display the results in Fig. 16. The difference in evolution leaves hardly any trace. Changing the freeze-out temperature has a larger effect. The small plateau in the distribution from hydrodynamics when $T_f = 140$ MeV has its origin in the first order phase transition and the mixed phase. However, the subsequent evolution

smooths this structure away as can be seen in the distribution with $T_f = 100$ MeV.

The different times of emission of photons and dileptons are manifested by comparison of the dilepton transverse momentum distribution (Fig. 17) and the photon distribution (Fig. 10). As we have remarked, the photon yields are dominated by the early hot stages of the evolution and show little dependence on freeze-out temperature. On the other hand, the dilepton yields in Fig. 17 clearly increase when the freeze-out temperature is lowered. The increase is more clearly seen in the transverse momentum distribution than in the mass distribution since the background is omitted in this figure.

VI. CONCLUSION

The expansion of matter described by hydrodynamics is rather similar to the expansion described by (coarse-grained) UrQMD. The transverse flow velocities in the central plane are nearly identical, but the temperature generally falls more slowly in UrQMD than in hydrodynamics. This is probably a consequence of the viscous nature of matter that is not accounted for in perfect fluid dynamics. The biggest difference between the two models occurs for the longitudinal flow velocity; its gradient along the beam axis is larger in UrQMD than in hydrodynamics. Since the initial conditions, so to speak, in UrQMD are a direct consequence of string dynamics there is no freedom to adjust them. It would be very interesting to modify the initial conditions in hydrodynamics to match those of UrQMD. It would also be very interesting to include viscosity and heat conduction in the fluid dynamical calculations to determine exactly how close the coarse-grained UrQMD results are to viscous flow.

Taking the coarse-grained UrQMD flow, temperature, and chemical potential fields as given, we computed the hadronic spectra in exactly the same way as in hydrodynamics. A freeze-out temperature of about 120 ± 10 MeV reproduces the experimental hadronic data of NA49 reasonably well. This should not be considered a substitute for the original hadronic spectra from UrQMD, but only serves to check that the coarse-graining procedure has not

severely distorted the results. Both hydrodynamics and UrQMD suggest that the matter created has a local temperature between 120 and 250 MeV for a period of about 15 fm/c with a transverse extent of about 10 fm.

The direct photon spectrum of WA98 is very well reproduced by a combination of perturbative QCD for the first hard scattering plus thermal radiation from either a hydrodynamic or an UrQMD expansion. It must be kept in mind that the pQCD calculation of direct photons is uncertain. In any case the high transverse momentum photons are sensitive to the early high-energy-density stage of the collision.

Both hydrodynamics and coarse-grained UrQMD give very similar numbers of low mass dileptons. The thermal emission rates seem to be rather robust since the different computations by Rapp et al. [29] and Eletsky *et al.* [30] give such similar results, although some uncertainty remains in the background “cocktail” contribution. These calculations tend to fall slightly below the data for the most central collisions in the invariant mass range 0.3–0.6 GeV, but the effect is less evident if the results are binned to conform to the experimental analysis. We suggest that further data are needed in order to decide whether a significant discrepancy with theory exists.

There is no doubt that the direct photon and low mass dilepton measurements require the formation of high density matter. Further data from central collisions at the SPS would be very useful and welcome. We also await the first results from RHIC on electromagnetic probes.

ACKNOWLEDGMENTS

This work was supported by the US Department of Energy grant DE-FG02-87ER40328.

REFERENCES

- [1] S. A. Bass, M. Belkacem, M. Bleicher, M. Brandstetter, L. Bravina, C. Ernst, L. Gerland, M. Hofmann, S. Hofmann, J. Konopka, G. Mao, L. Neise, S. Soff, C. Spieles, H. Weber, L. A. Winckelmann, H. Stöcker, W. Greiner, Ch. Hartnack, J. Aichelin and N. Amelin, *Prog. Part. Nucl. Phys.* **41**, 225 (1998).
- [2] M. Bleicher, E. Zabrodin, C. Spieles, S. A. Bass, C. Ernst, S. Soff, L. Bravina, M. Belkacem, H. Weber, H. Stöcker and W. Greiner, *J. Phys. G: Nucl. Part. Phys.* **25**, 1859 (1999).
- [3] J. Sollfrank, P. Huovinen, M. Kataja, P. V. Ruuskanen, M. Prakash and R. Venugopalan, *Phys. Rev. C* **55**, 392 (1997).
- [4] J. Sollfrank, P. Huovinen and P. V. Ruuskanen, *Eur. Phys. J. C* **6**, 525 (1999).
- [5] T. Peitzmann and M. H. Thoma, hep-ph/0111114.
- [6] R. Rapp and J. Wambach, *Adv. Nucl. Phys.* **25**, 1 (2000).
- [7] M. Belkacem, M. Brandstetter, S. A. Bass, M. Bleicher, L. Bravina, M. I. Gorenstein, J. Konopka, L. Neise, C. Spieles, S. Soff, H. Weber, H. Stöcker and W. Greiner, *Phys. Rev. C* **58**, 1727 (1998).
- [8] P. Huovinen, P. V. Ruuskanen and J. Sollfrank, *Nucl. Phys. A* **650**, 227 (1999).
- [9] P. Huovinen and M. Prakash, *Phys. Lett. B* **450**, 15 (1999).
- [10] M. Bleicher, C. Spieles, C. Ernst, L. Gerland, S. Soff, L. Neise, H. Stöcker, W. Greiner and S. A. Bass, *Phys. Lett. B* **447**, 227 (1999).
- [11] S. Soff, D. Zschesche, M. Bleicher, C. Hartnack, M. Belkacem, L. Bravina, E. Zabrodin, S. A. Bass, H. Stöcker and W. Greiner, *J. Phys. G: Nucl. Part. Phys.* **27**, 449 (2001).
- [12] P. G. Jones *et al.* [NA49 Collaboration], *Nucl. Phys. A* **610**, 188c (1996).

- [13] M. M. Aggarwal *et al.* [WA98 Collaboration], Phys. Rev. Lett. **85**, 3595 (2000).
- [14] C. Y. Wong and H. Wang, Phys. Rev. C **58**, 376 (1998).
- [15] C. Gale, Nucl. Phys. A **698**, 143c (2002).
- [16] A. Dumitru, L. Frankfurt, L. Gerland, H. Stöcker and M. Strikman, Phys. Rev. C **64**, 054909 (2001).
- [17] D. K. Srivastava and B. Sinha, Phys. Rev. C **64**, 034902 (2001); J. Alam, S. Sarkar, T. Hatsuda, T. K. Nayak and B. Sinha, *ibid.* **63**, 021901 (2001); J. Alam, P. Roy, S. Sarkar and B. Sinha, nucl-th/0106038; D. Y. Peressounko and Y. E. Pokrovsky, hep-ph/0009025; A. K. Chaudhuri, nucl-th/0012058; K. Gallmeister, B. Kampfer and O. P. Pavlenko, Phys. Rev. C **62**, 057901 (2000); F. D. Steffen and M. H. Thoma, Phys. Lett. B **510**, 98 (2001).
- [18] P. Huovinen, P. V. Ruuskanen and S. S. Räsänen, nucl-th/0111052.
- [19] J. Kapusta, P. Lichard and D. Seibert, Phys. Rev. D **44**, 2774 (1991).
- [20] H. Nadeau, J. Kapusta and P. Lichard, Phys. Rev. C **45**, 3034 (1992).
- [21] L. Xiong, E. Shuryak and G. E. Brown, Phys. Rev. D **46**, 3798 (1992).
- [22] P. Arnold, G. D. Moore and L. G. Yaffe, JHEP **0111**, 057 (2001); JHEP **0112** (2001).
- [23] A. Dumitru, M. Bleicher, S. A. Bass, C. Spieles, L. Neise, H. Stöcker and W. Greiner, Phys. Rev. C **57**, 3271 (1998).
- [24] B. Lenkeit *et al.* [CERES Collaboration], Nucl. Phys. A **661**, 23 (1999).
- [25] C. Voigt, Doctoral Thesis, University of Heidelberg, 1998.
- [26] B. Lenkeit, Doctoral Thesis, University of Heidelberg, 1998.
- [27] C. Gale and P. Lichard, Phys. Rev. D **49**, 3338 (1994).

- [28] P. Lichard, Phys. Rev. D **49**, 5812 (1994).
- [29] R. Rapp, G. Chanfray and J. Wambach, Nucl. Phys. **A617**, 472 (1997); R. Rapp, Phys. Rev. C **63**, 054907 (2001).
- [30] V. L. Eletsky, M. Belkacem, P. J. Ellis and J. I. Kapusta, Phys. Rev. C **64**, 035202 (2001).
- [31] D. K. Srivastava and J. I. Kapusta, Phys. Rev. C **48**, 385 (1993).
- [32] R. Rapp and J. Wambach, Eur. Phys. J A **6**, 415 (1999).

FIGURES

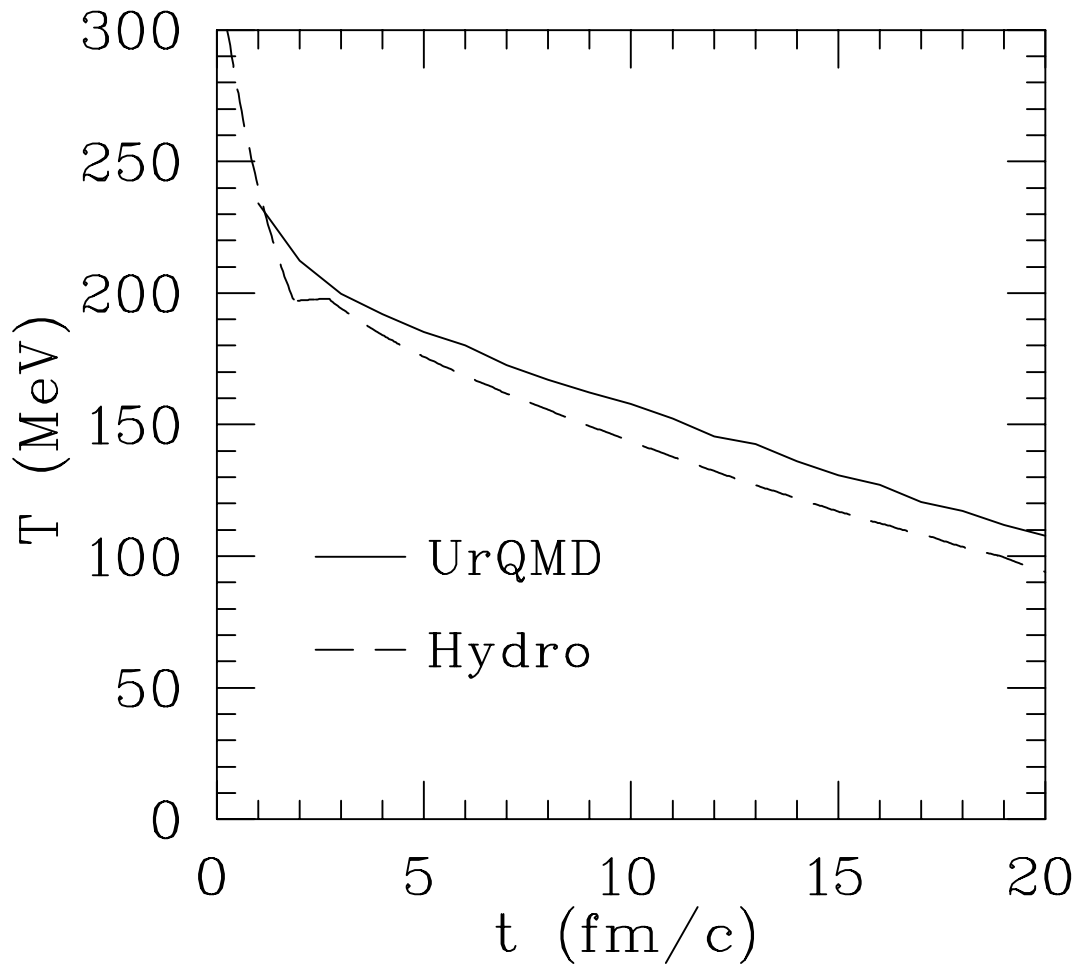


FIG. 1. The temperature as a function of local time at the origin in the UrQMD model (solid curve) and the hydrodynamic model (dashed curve).

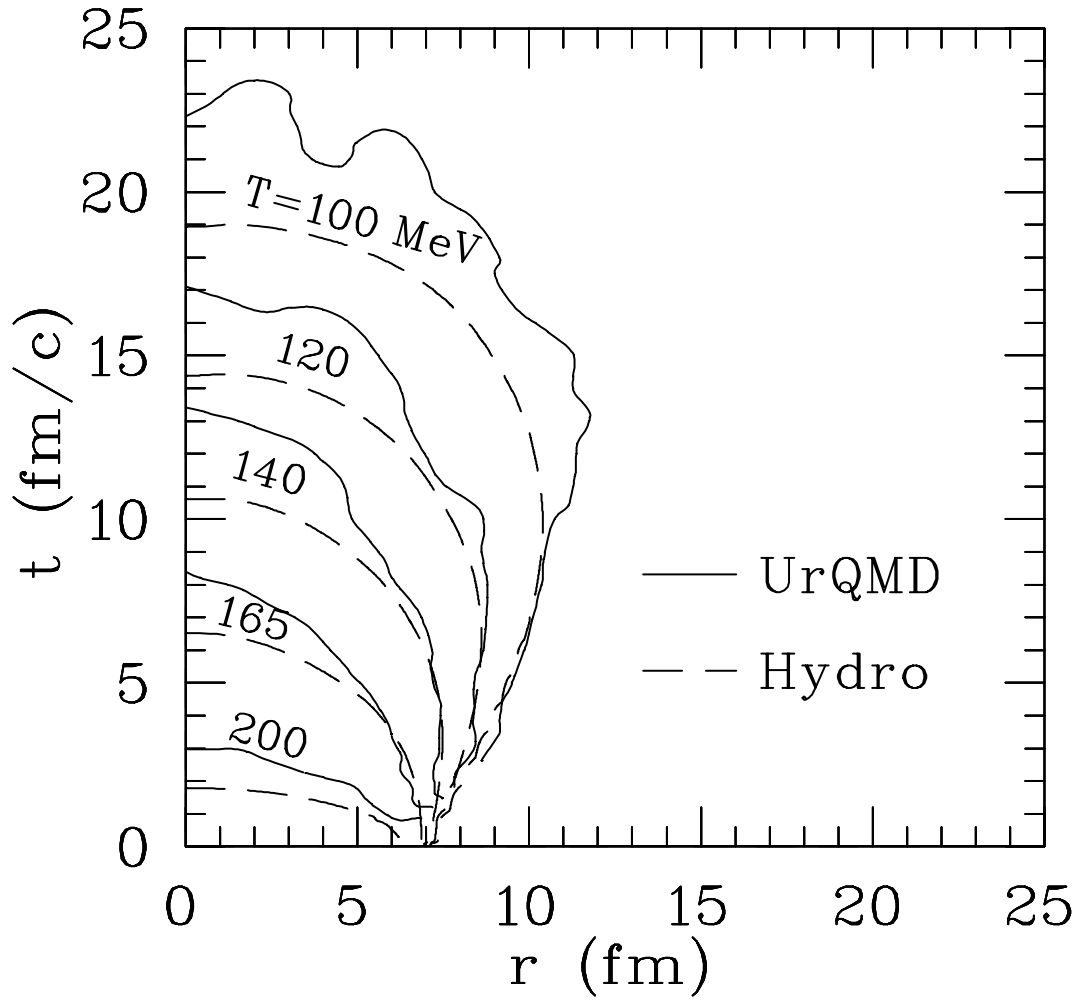


FIG. 2. Temperature contours in local time and cylindrical radius in the central transverse plane for the UrQMD model (solid curves) and the hydrodynamic model (dashed curves).

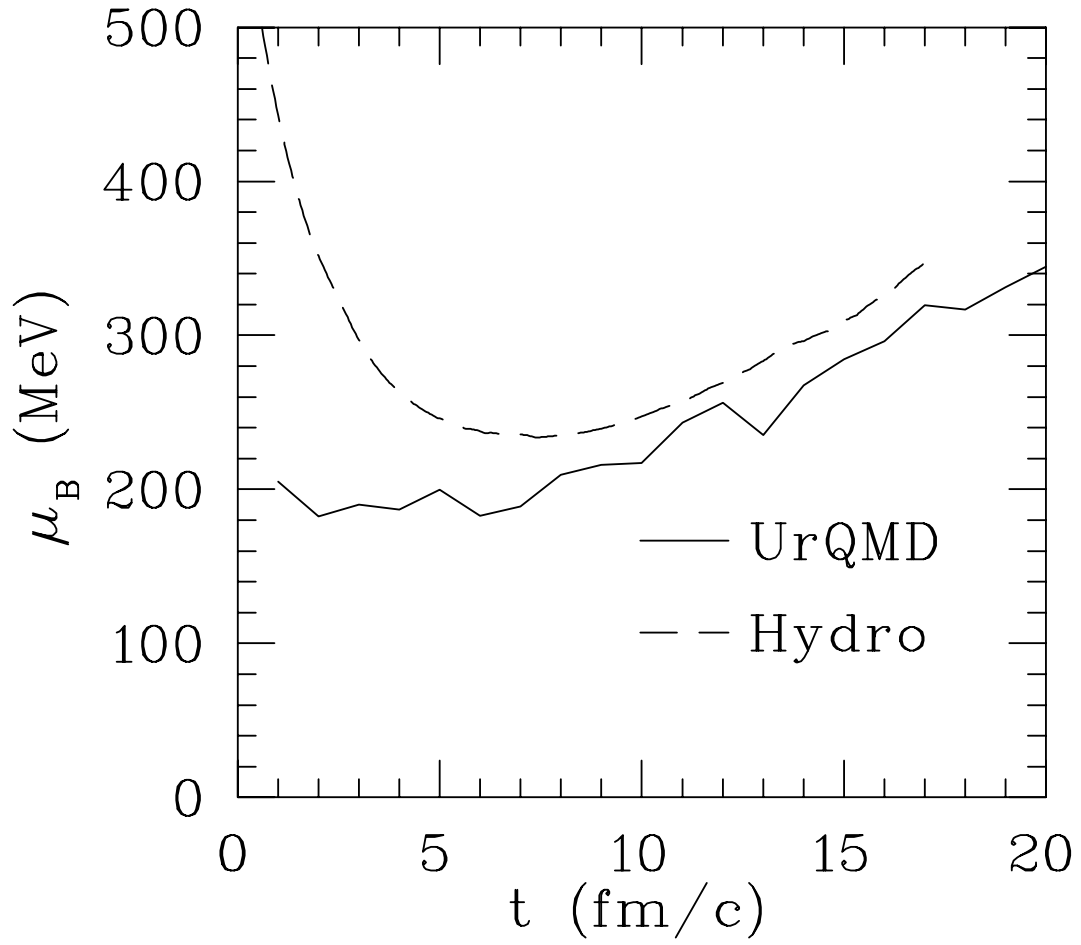


FIG. 3. The time evolution of the baryon chemical potential at the origin in the UrQMD model (solid curve) and the hydrodynamic model (dashed curve).

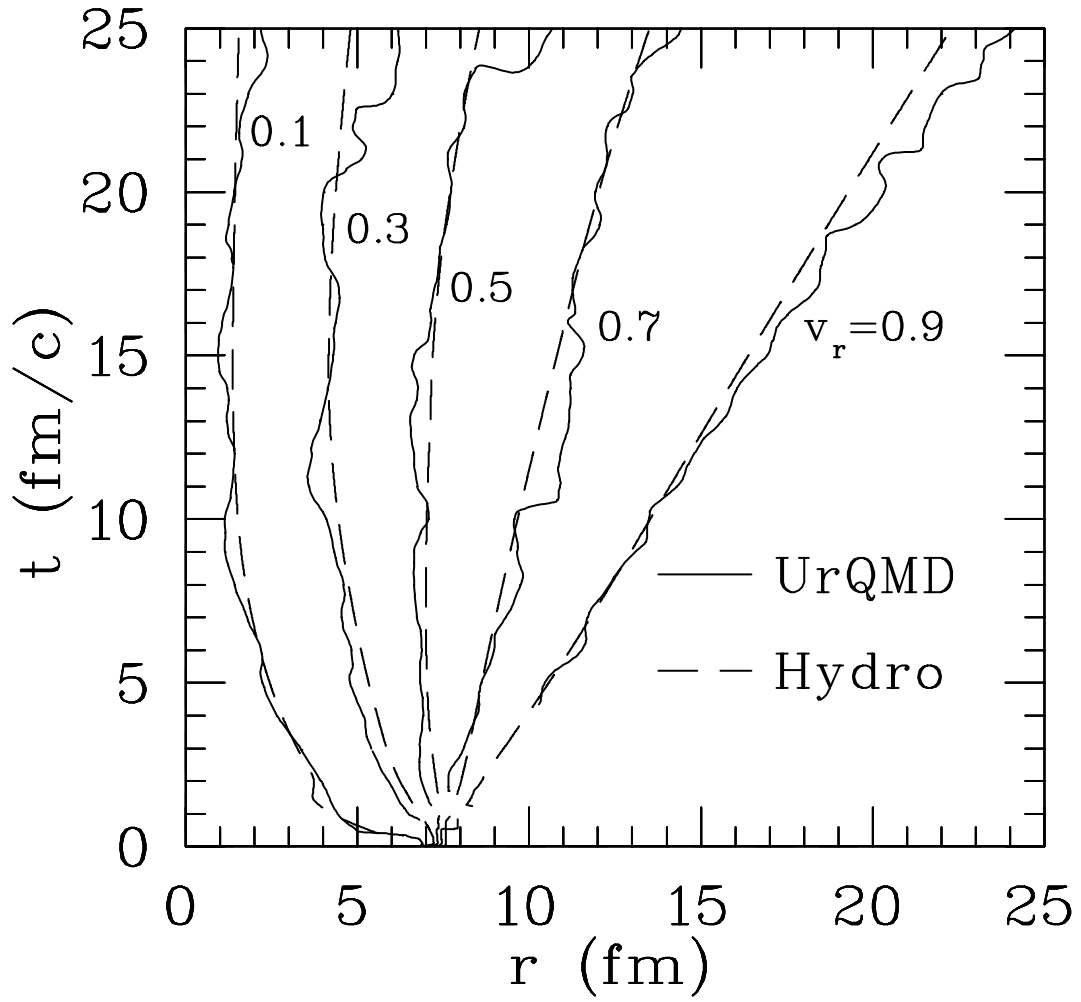


FIG. 4. Contours of equal radial flow velocity as a function of local time and cylindrical radius in the central transverse plane for the UrQMD model (solid curves) and the hydrodynamic model (dashed curves).

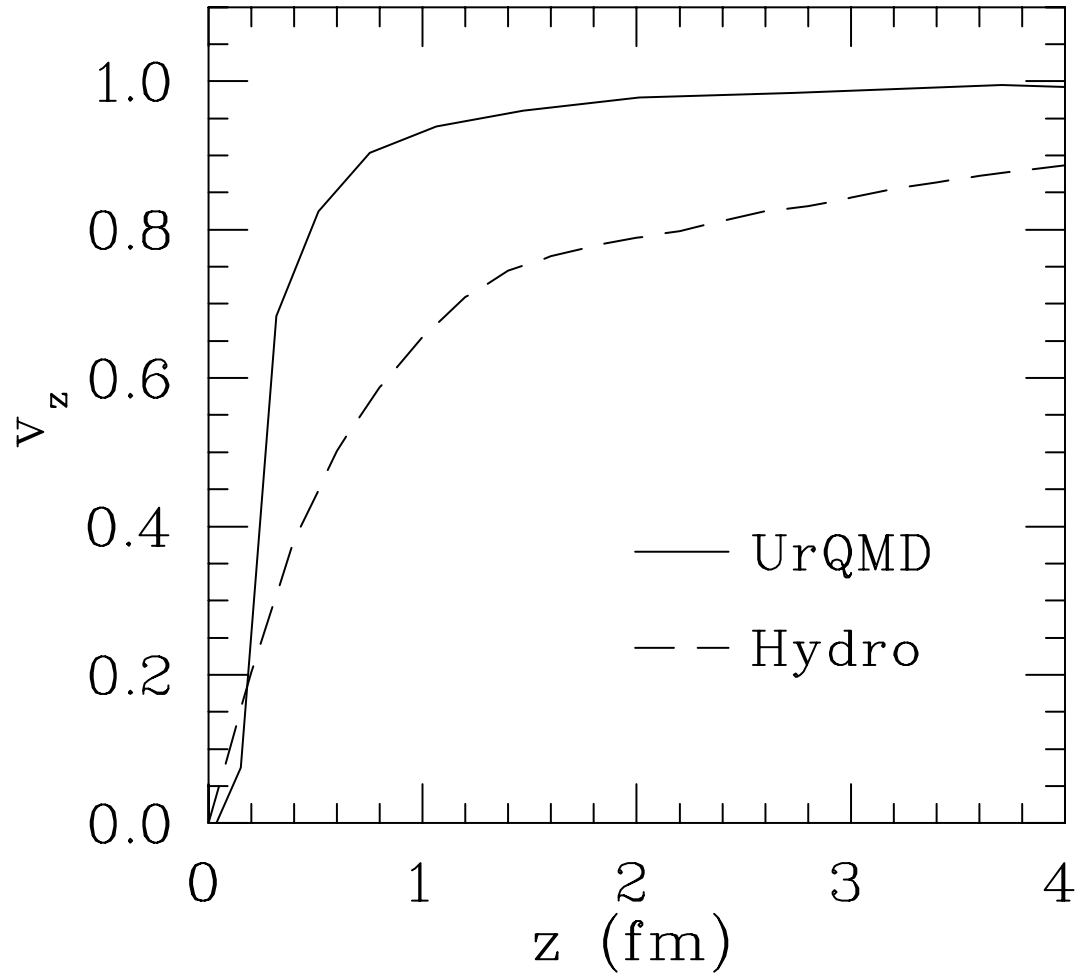


FIG. 5. The initial velocity distribution along the beam axis in the UrQMD model (solid curve) and the hydrodynamic model (dashed curve).

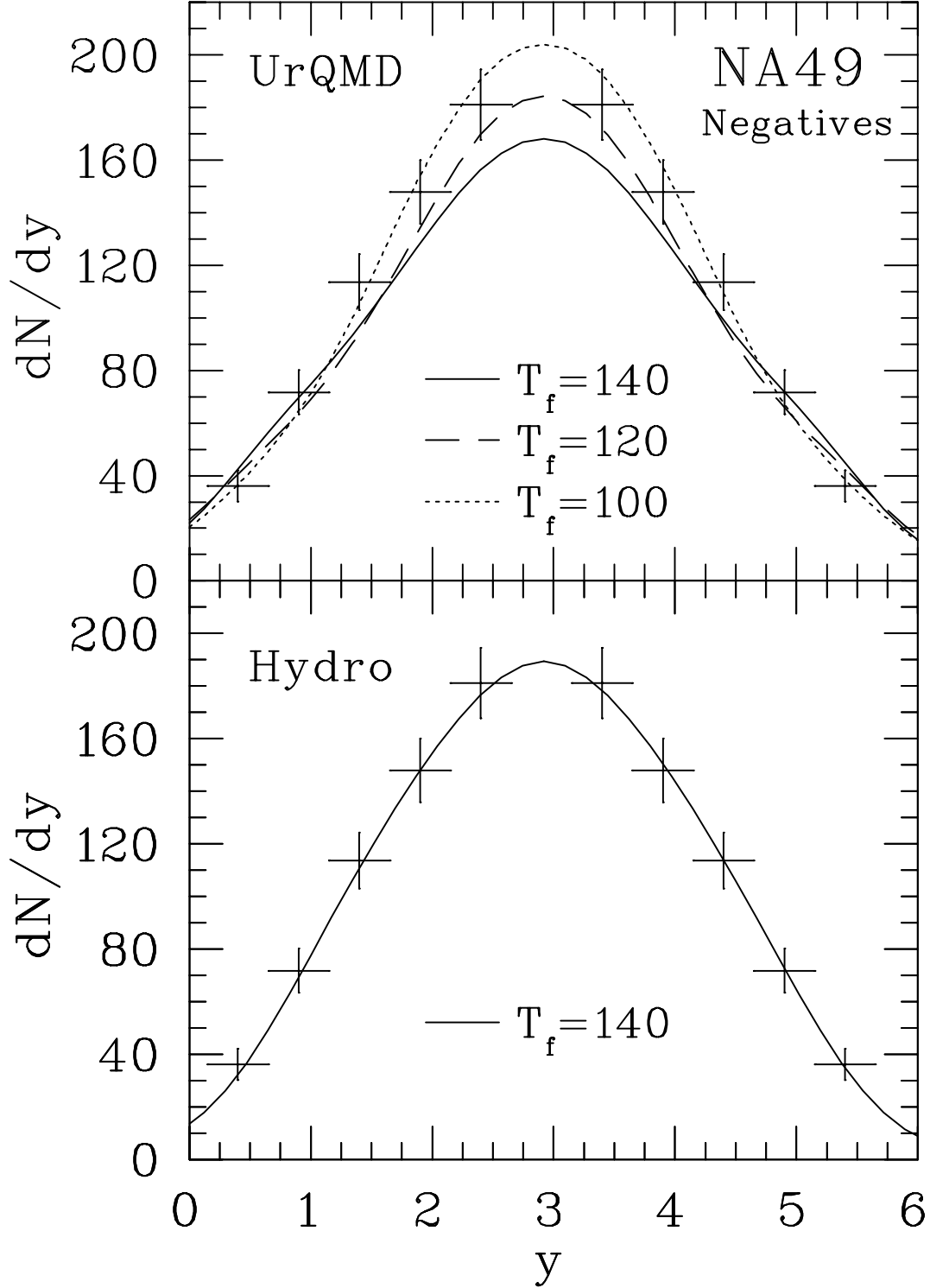


FIG. 6. The rapidity distribution of negatively charged hadrons. Upper panel: UrQMD for various freeze-out temperatures; lower panel: hydrodynamic model; data: NA49 collaboration [12].

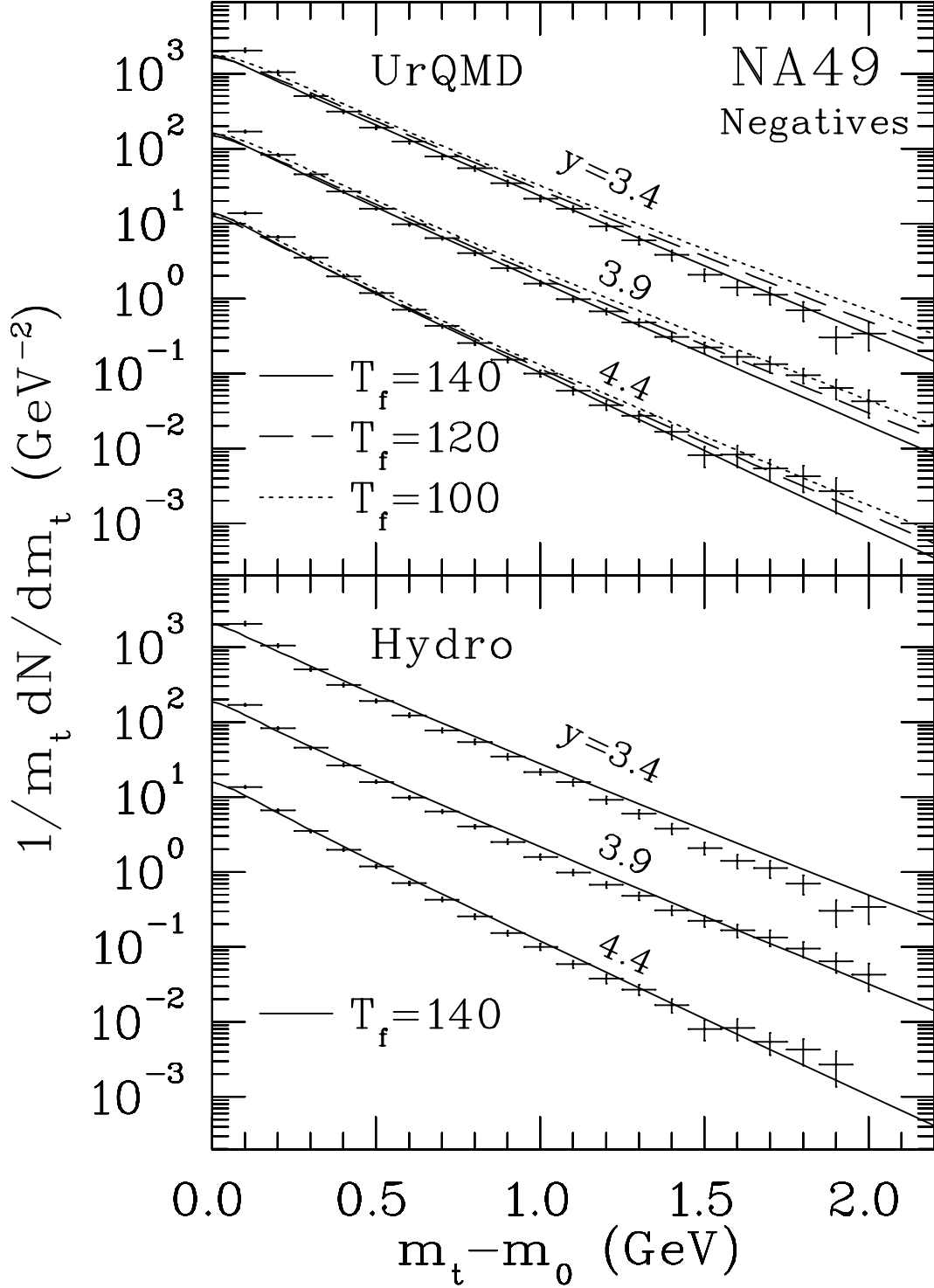


FIG. 7. The transverse mass distributions of negatively charged hadrons at rapidities of 3.4, 3.9 and 4.4. Upper panel: UrQMD for various freeze-out temperatures; lower panel: hydrodynamic model; data: NA49 collaboration [12].

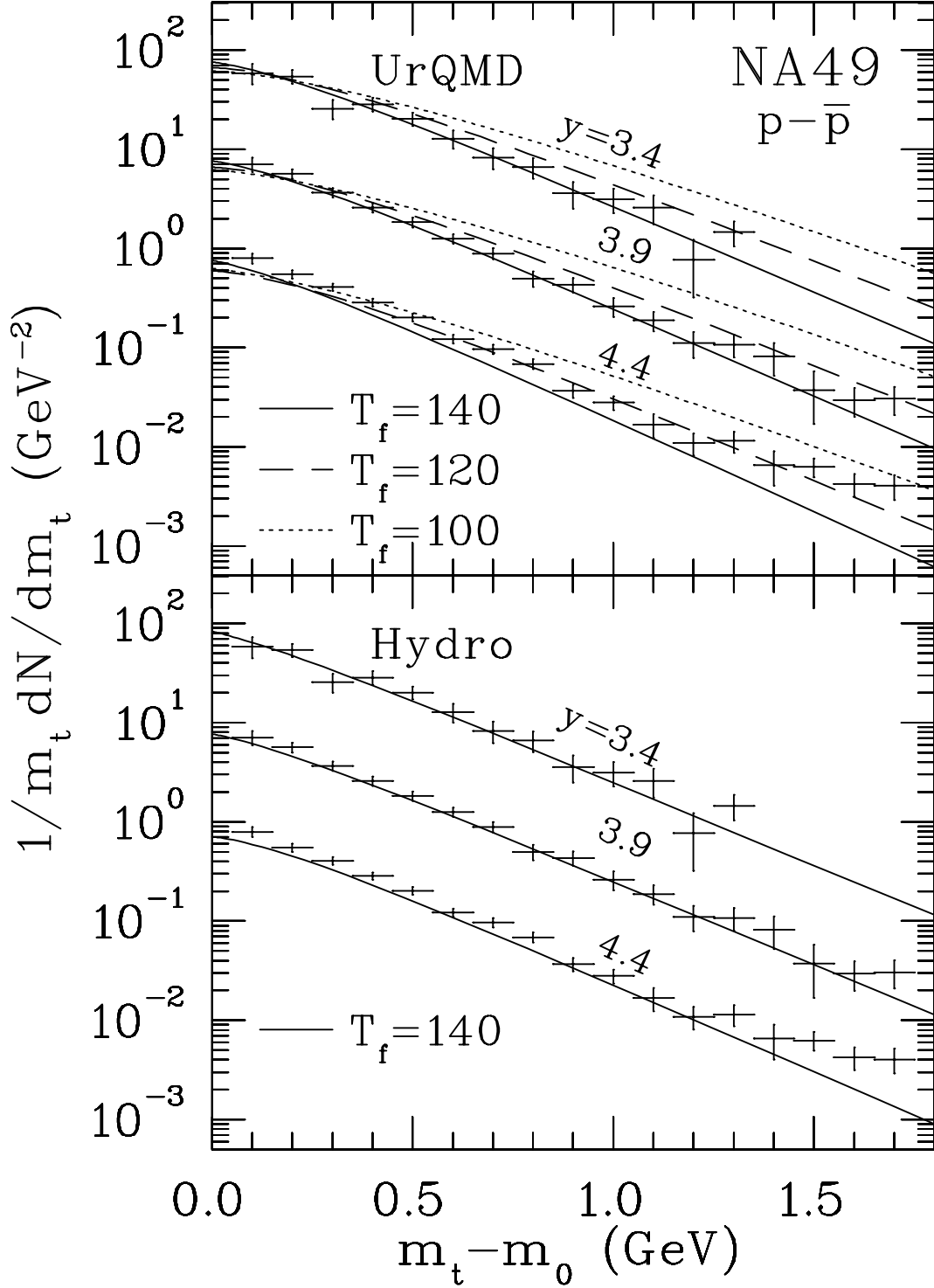


FIG. 8. The net proton spectra at rapidities of 3.4, 3.9 and 4.4. Upper panel: UrQMD for various freeze-out temperatures; lower panel: hydrodynamic model; data: NA49 collaboration [12].

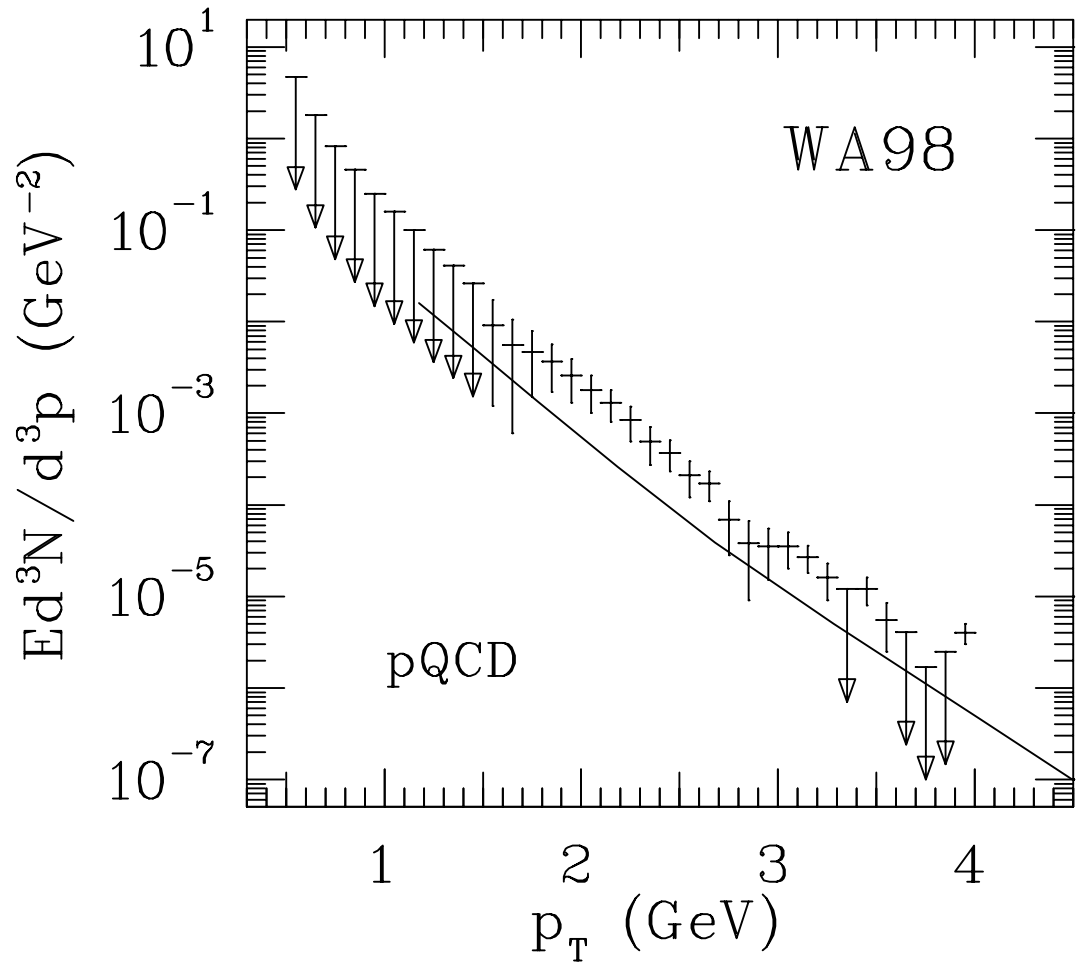


FIG. 9. Photon spectrum from Pb-Pb collisions at 158 A GeV by the WA98 collaboration [13] compared to a perturbative QCD calculation [14].

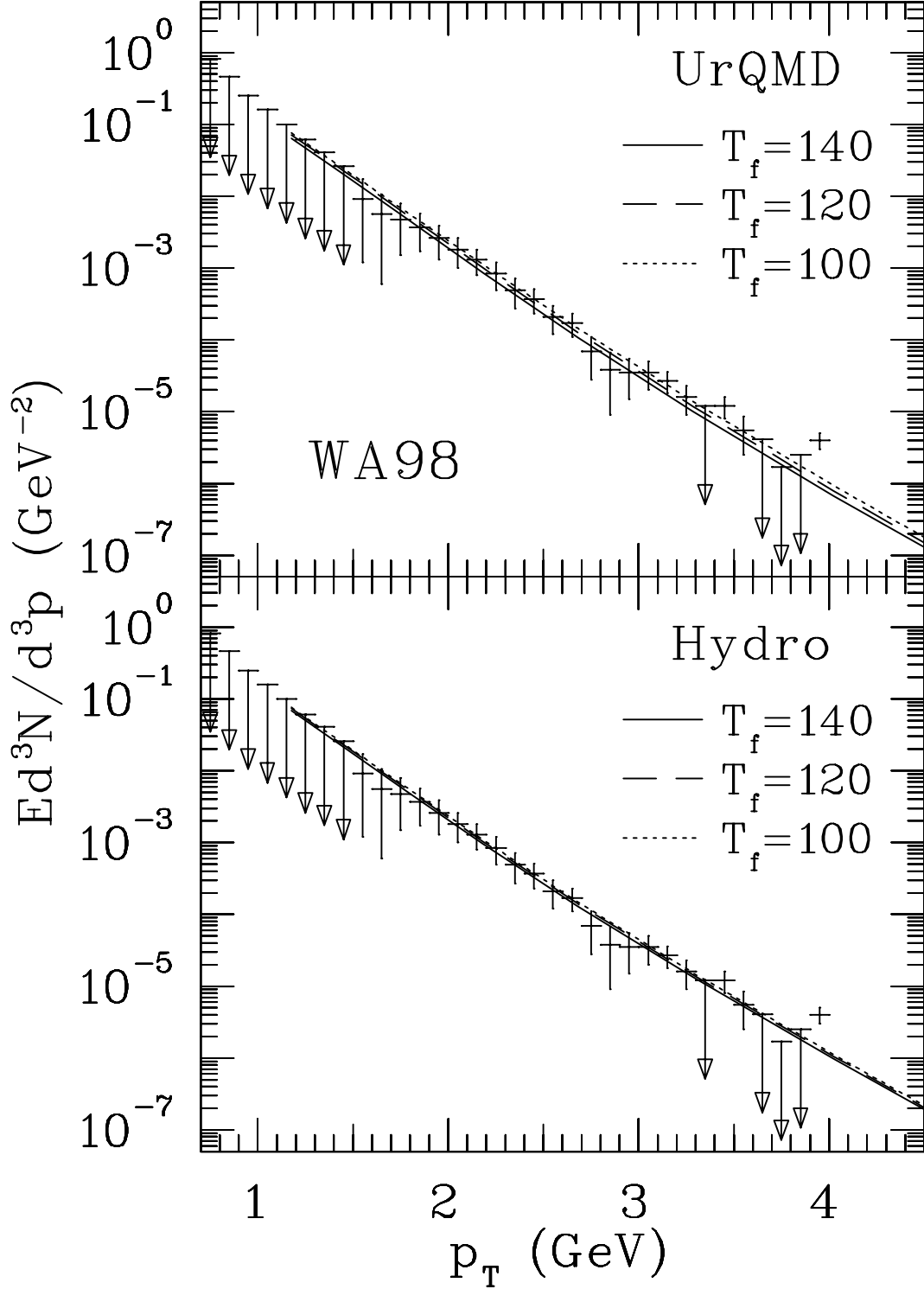


FIG. 10. Comparison of the WA98 photon spectrum [13] to the predictions of the UrQMD model (upper panel) and the hydrodynamic model (lower panel) at several freeze-out temperatures.

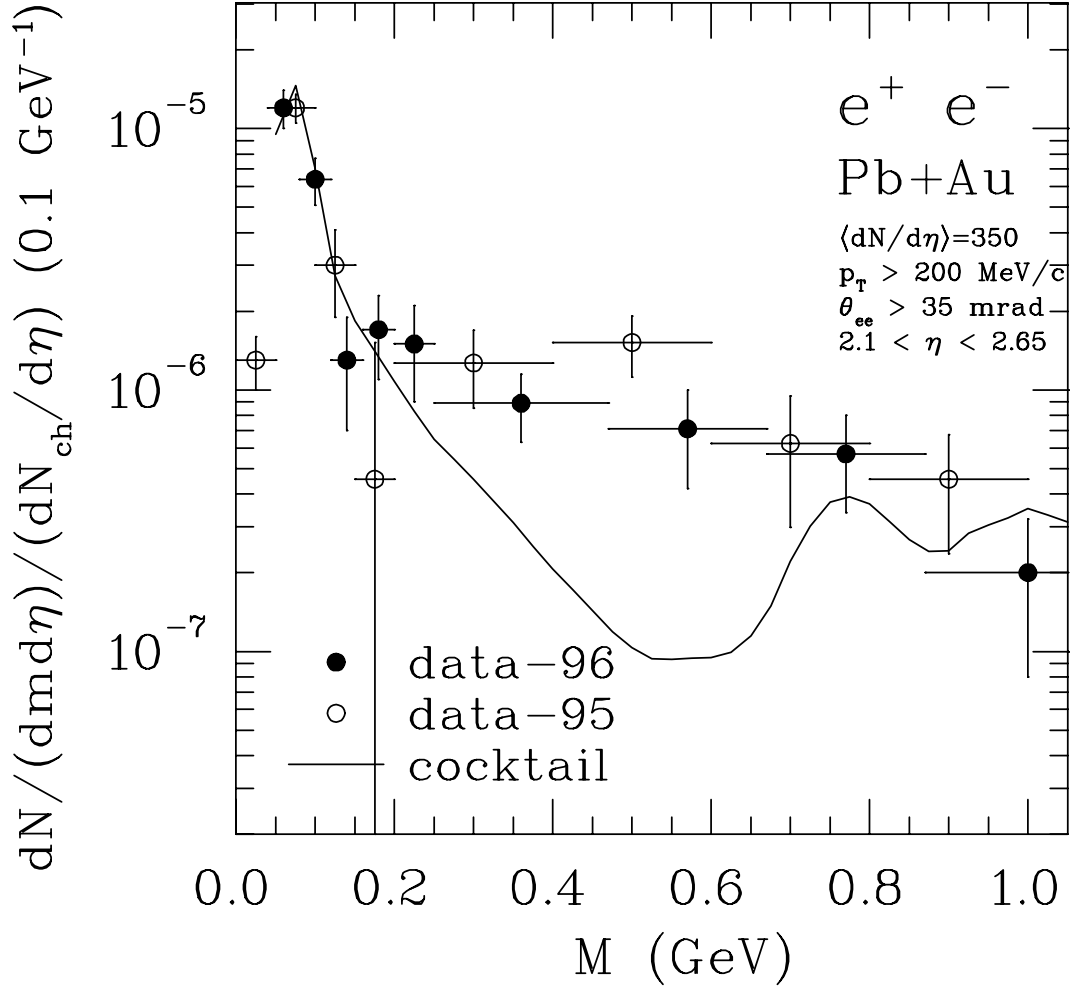


FIG. 11. Comparison of the dilepton data for Pb-Au collisions at 158 A GeV ('95 data Ref. [25], '96 data Ref. [26]) with the contribution from the decay of hadrons after freezeout.

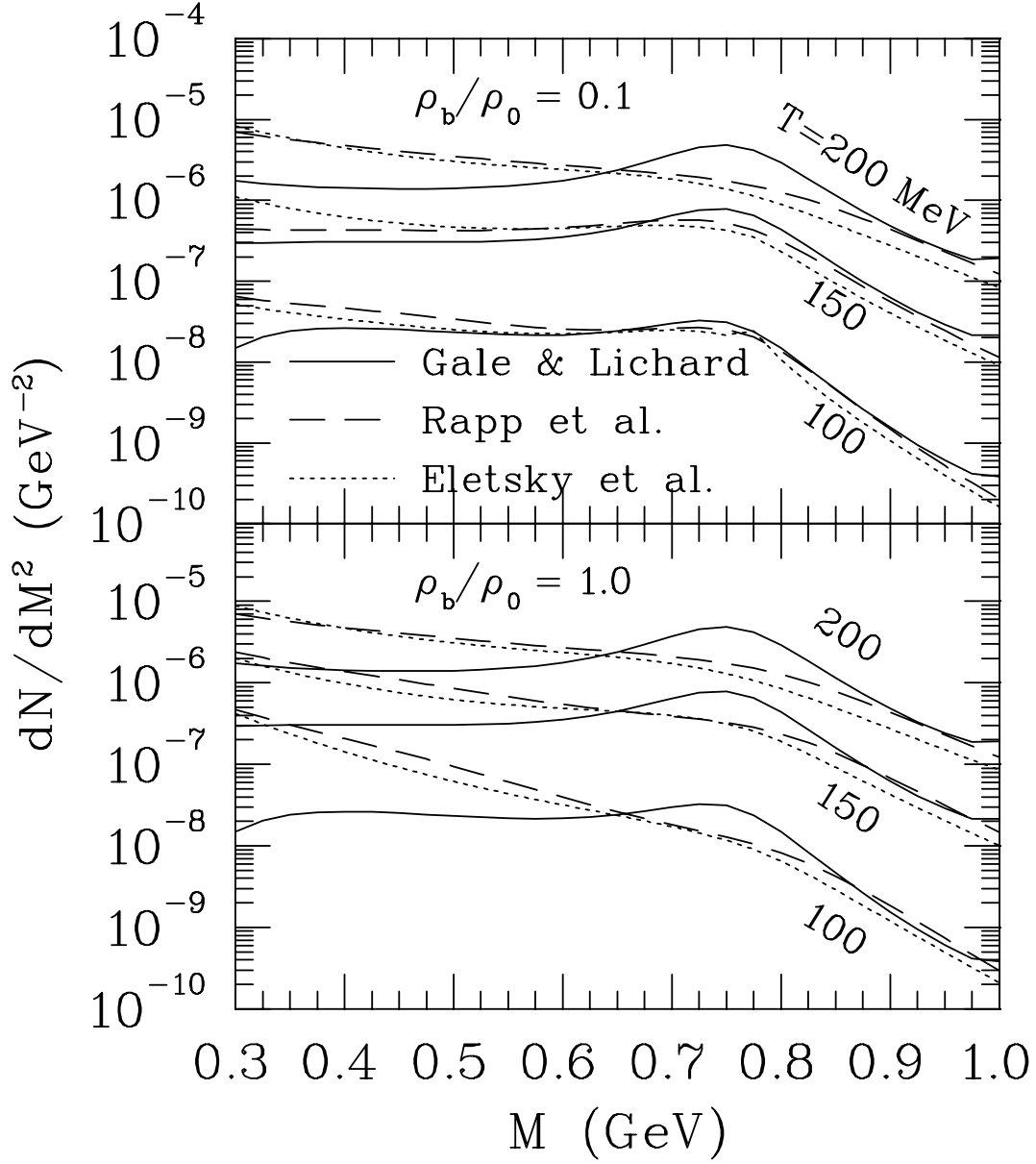


FIG. 12. Thermal dilepton emission rates computed by Gale and Lichard [27,28], Rapp *et al.* [29] and Eletsky *et al.* [30] at various temperatures. The baryon densities are fixed at 1/10 (upper panel) and 1 (lower panel) times the equilibrium density of cold nuclear matter.

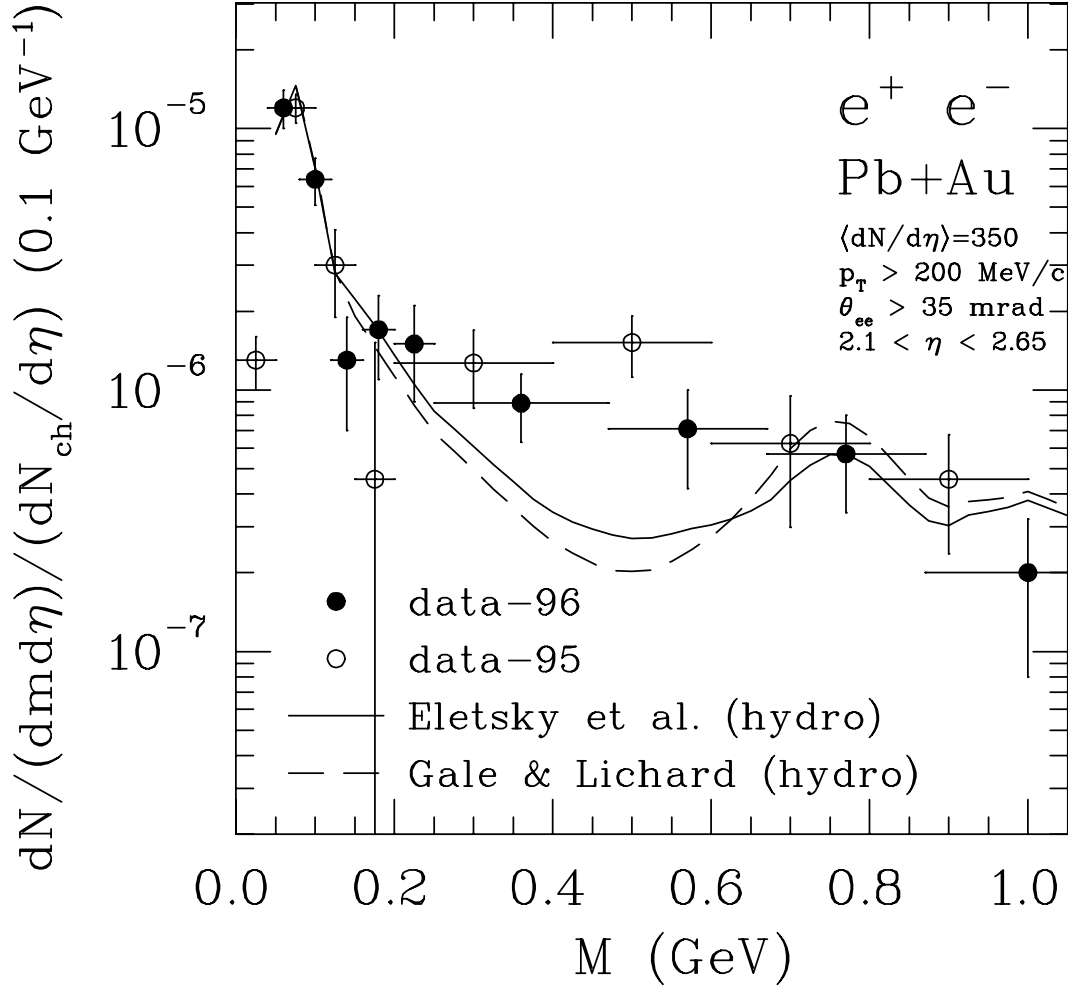


FIG. 13. Comparison of the dilepton data [25,26] with hydrodynamic predictions using the emission rates of Gale and Lichard [27,28] (dashed curve) and Eletsky *et al.* [30] (solid curve). The latter employs medium-modified hadrons.

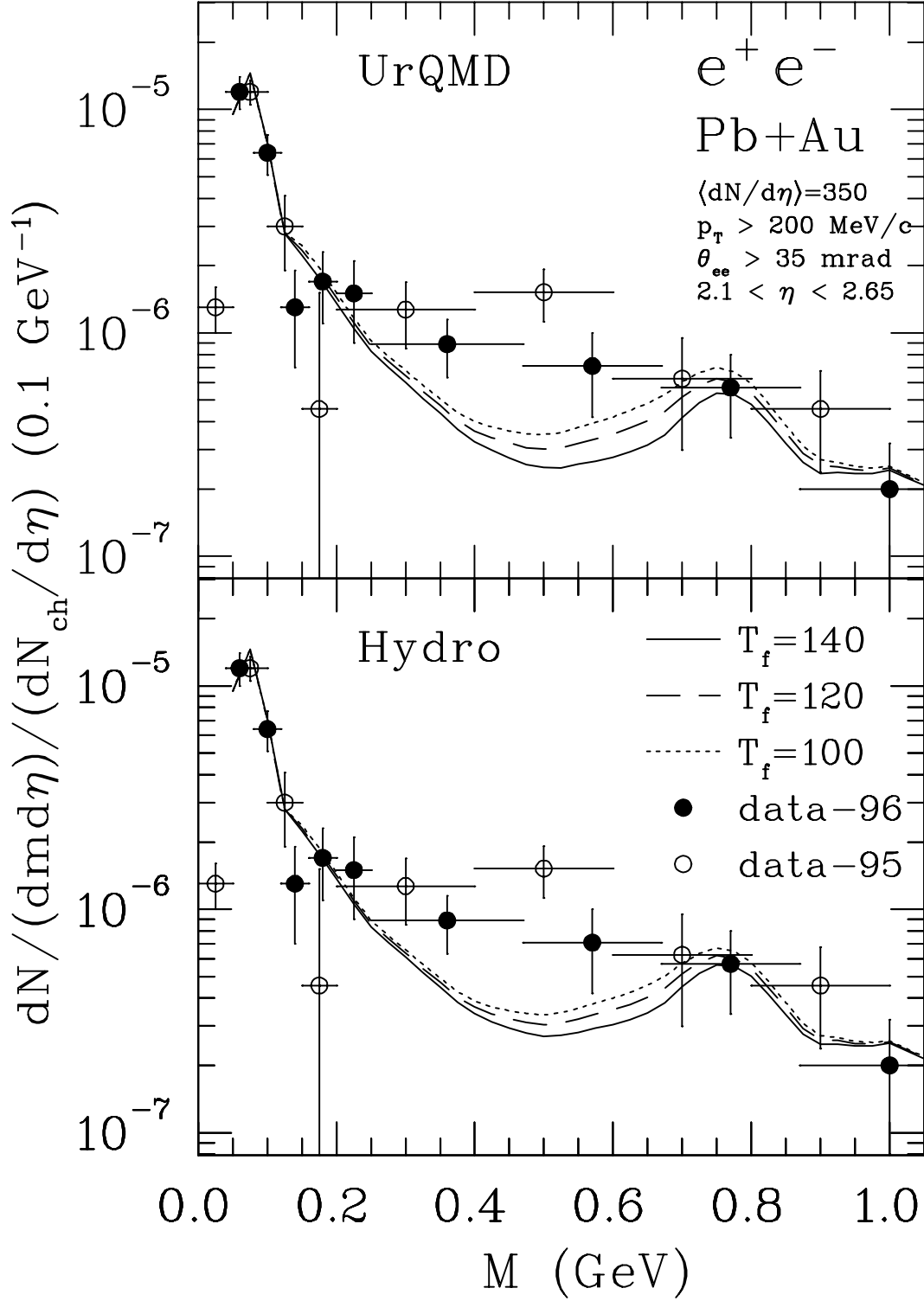


FIG. 14. Comparison of the dilepton data [25,26] with predictions of the UrQMD model (upper panel) and the hydrodynamic model (lower panel) at several freeze-out temperatures.

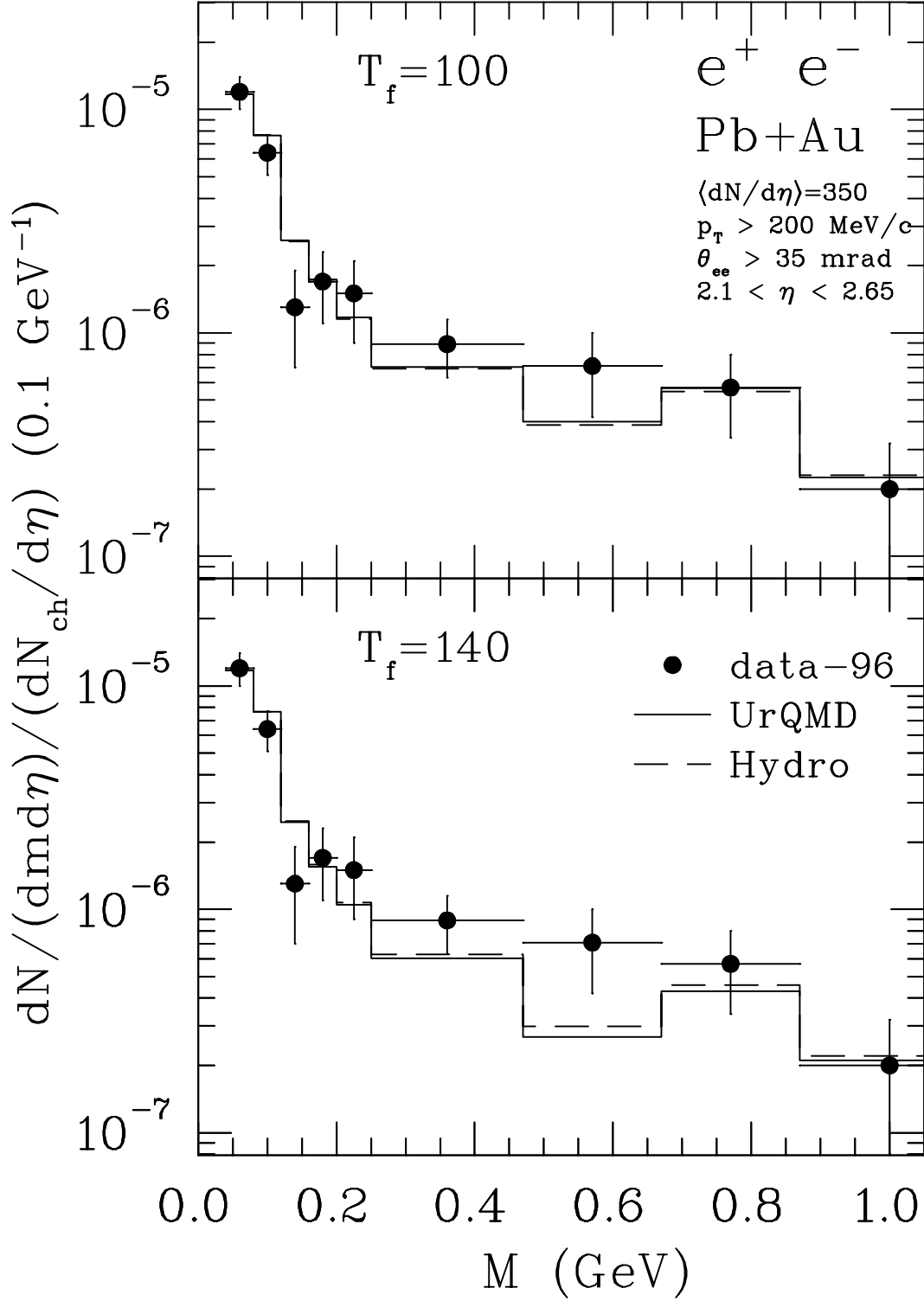


FIG. 15. Comparison of the dilepton data [26] with binned predictions of the UrQMD model (solid lines) and the hydrodynamic model (dashed lines) at two freeze-out temperatures.

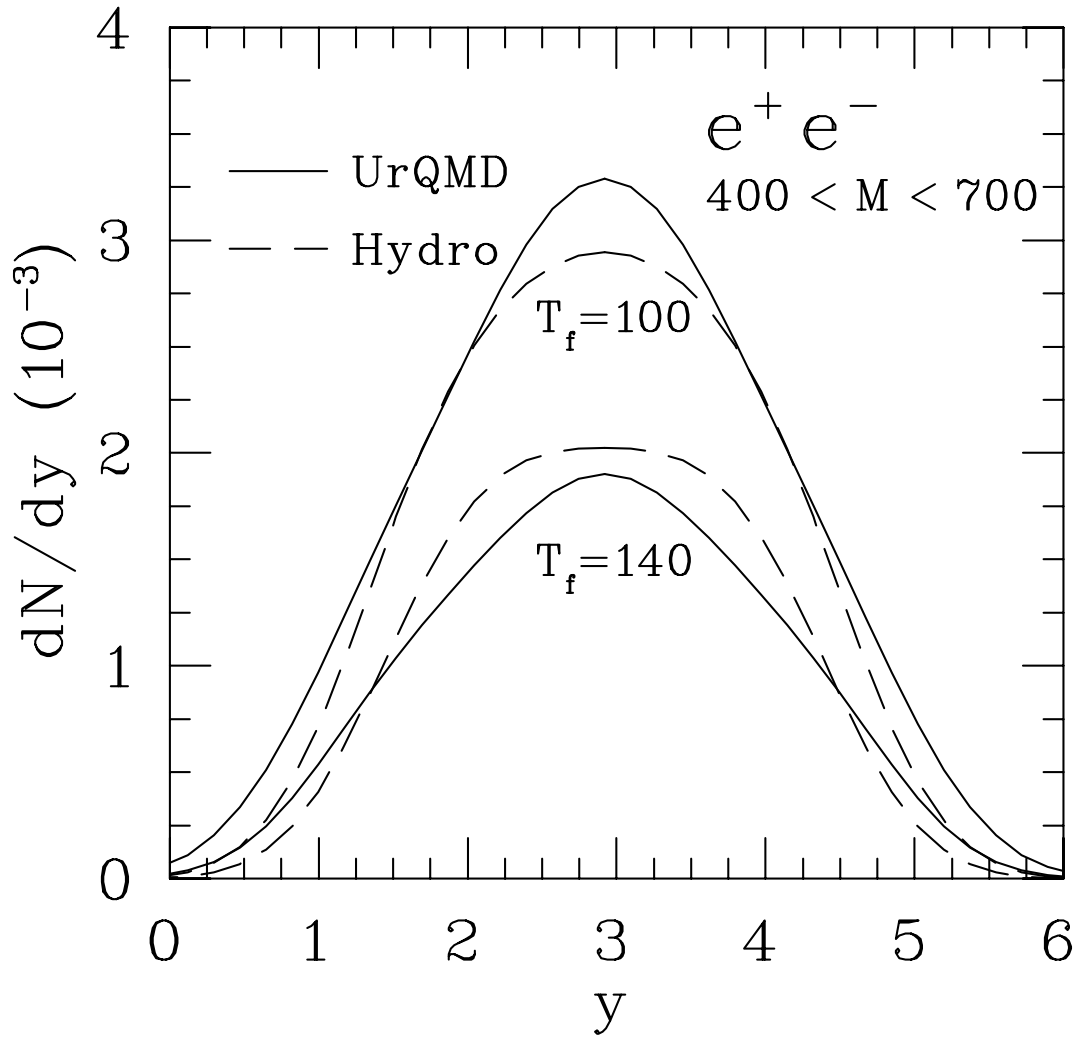


FIG. 16. Rapidity distributions of dileptons in the UrQMD model (solid curves) and hydrodynamic model (dashed curves) for two freeze-out temperatures.

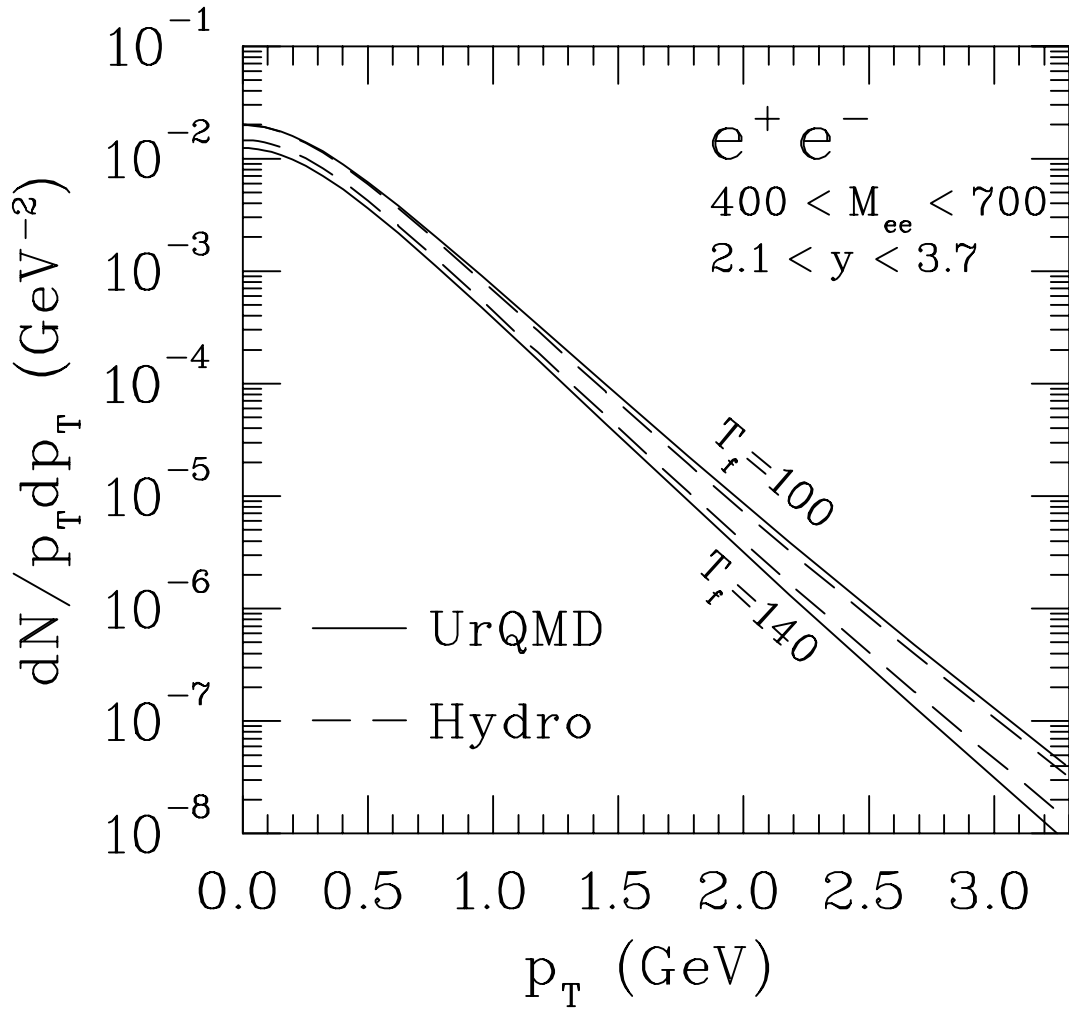


FIG. 17. The transverse momentum distributions at mid-rapidity in the UrQMD model (solid curves) and the hydrodynamic model (dashed curves) for two freeze-out temperatures.